

# Experimental Investigation of Nonlinear Vibration Isolator with Fluidic Actuators (NLVIFA)

S. Sivakumar<sup>1,\*</sup> and L. Jayakumar<sup>2</sup>

<sup>1</sup>Department of Automobile Engineering, Arunai Engineering College, Tiruvannamalai, 606603, India

<sup>2</sup>Department of Mechanical Engineering, Arunai Engineering College, Tiruvannamalai, 606603, India

\*Corresponding Author: S. Sivakumar. Email: sivakumarsolaiachari@gmail.com.

**Abstract:** This paper elaborates a nonlinear fluidic low frequency vibration isolator designed with the characteristics of quasi-zero stiffness (QZS). The existing model of QZS vibration isolator enhances amplitude of vibration and attenuating vibration frequencies. This concern with displacement plays a vital role in the performance and instability of oblique spring setup reduces the isolator performance in horizontal non-nominal loads, in this accordance; this paper associates double acting hydraulic cylinder (fluidic actuators in short) in oblique and helical coil spring. An approximate expression of unique analytical relationship between the stiffness of vertical spring and bulk modulus of the fluid is derived for Quasi – Zero Stiffness Non-Linear Vibration Isolator with Fluidic Actuators (NLVIFA in short) system and the force transmissibility is formulated and damping ratio are discussed for characteristic analysis. Modal analysis carried out and compared with analytical results and an experimental prototype is developed and investigated. The performance of the NLVIFA reduces the external embarrassment more at low frequencies and the series of experimental studies showing that the soft nonlinearity causes limitation in the resonant frequency thereupon the isolation will be enhanced and NLVIFA greatly outperform some other type of nonlinear isolators.

**Keywords:** Quasi zero stiffness; vibration; nonlinear isolation; fluidic actuator

## 1 Introduction

In every dynamic systems an unwanted vibrations are one of the main causes to promote harmful effects such as fatigue or failure and diminishing the performance [1]. Passive isolation techniques are generally approaches to reduce the effect of unwanted vibrations [2]. Isolation performance can be improved by using nonlinearity with damping and stiffness [3]. An active frequency range for a linear vibration isolator is often attenuated by the base stiffness to support a static load. Therefore, it cannot control the dynamic vibration frequency drastically. It can be enhanced by employing a nonlinear structure incorporating limited stiffness elements as dynamic stiffness is less than the static stiffness- was proposed by Ibrahim [4]. The unbalanced motor spectrum and density given by [5] and The power spectrum of motor frequency of rotor misalignment and eccentricity causes non-nominal loads [6], effects to reduce machinery life span and gives worse experience to human beings. To reduce this harmful non nominal vibration into smooth the proposed system introduced. Generally the QZS

vibration isolator consists of two adjustment mechanisms. The oblique adjustment is designed to match the geometric ratio with the stiffness ratio so that likely zero stiffness can be achieved under imperfect condition. The vertical adjustment is used to maintain the equilibrium position so that isolation is applicable to different loads [7]. Most of the studies have intensified on the reduction of the isolator's natural frequency by using various types of absorbers introduced in various Directions. Such as helical coil springs placed in oblique and vertical directions [7, 8], Euler's buckled beam fixed in horizontal direction and helical coil spring in vertical direction [9] and Magnetic repulsive force with initial gap settings on horizontal direction and helical coil spring in vertical direction [10]. From these existing models the nonlinear vibration greatly controlled and enhancement of vibration isolation initiated, but it is difficult to providing stability of helical coil springs and isolation performance in oblique direction, compactness of the entire system will be large due to helical coil spring provisions and the main thing is that the existing nonlinear systems are limited with various static loads which means the applicable performance stands with only on designed static loading conditions. Considering an expeditious growth of industrial engineering technology the emphasis for vibration isolation increasing. It can be improved by adopting new technology by reviewing the recent advances in nonlinear isolation. A typical form of a Quasi Zero Stiffness Vibration isolator was designed with fluidic actuators namely NLVIFA. In order to improve the performance in isolating the non-nominal frequency vibration and performance under various static load conditions, it is proposed to use fluidic actuators on oblique and vertical supports. The focus of this paper is to furnish the theoretical and experimental analysis of NLVIFA vibration isolator to acquire the requirements of an unbalanced system to balance and exhibit the time delayed active absorption and the enactment of self active isolation with various static loads.

## **2 QZS-FA Vibration Isolator**

The QZS-VIFA vibration isolator setup consists of a vertical base actuator which can actuate with respect to two oblique actuator's movements. The vertical and oblique actuators are cross-connected to achieve the quasi zero stiffness at the equilibrium position.

### **2.1 Isolator Elements**

The vibration isolator setup is designed with capable of withstanding a non-linear dynamic load. The isolator equipped with the following elements (i) Isolator frame, (ii) Fluidic actuator - lateral (FA in short) two nos., (iii) FA – vertical base (BA in short), (iv) Helical coil spring (HCS), (v) Load-base, (vi) Spring-base and (vii) pressurized fluid carrying hose for actuators connections.

### **2.2 Physical Structure of QZS-FA Vibration Isolator**

It is contrived by double acting hydraulic cylinder (in short fluidic actuator) as working member. The C-section channel frame as similar to [9] structure having two vertical columns and the FA pivotally joined at the ends of each vertical column since it is impractical to extend both FA in horizontal. The FA piston rod ends connected and pivotally hanging the load base which opting the external unbalanced loads.

Fluidic hose connects outward and inward ports of cylinder 1 and cylinder 2 in parallel as inward bus and outward bus. And these buses cross-connected (inward to outward vice versa) with BA. At the top of the BA, a plate called spring-base attached, in between the spring base and load base a helical coil spring provided to enhance the isolation performance. A two-dimensional Sketch of proposed NLVIFA shown in Fig. 1.

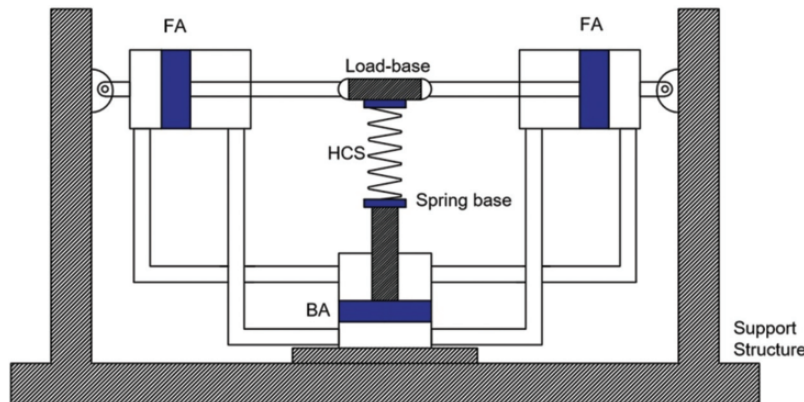


**Figure 1:** 2D - Sketch of QZS - FA vibration isolator

### 3 Analytical Investigations

The QZS-FA Vibration isolator system acting while under being applied force and excited force are illustrated in Fig. 2(a) and (b) respectively.

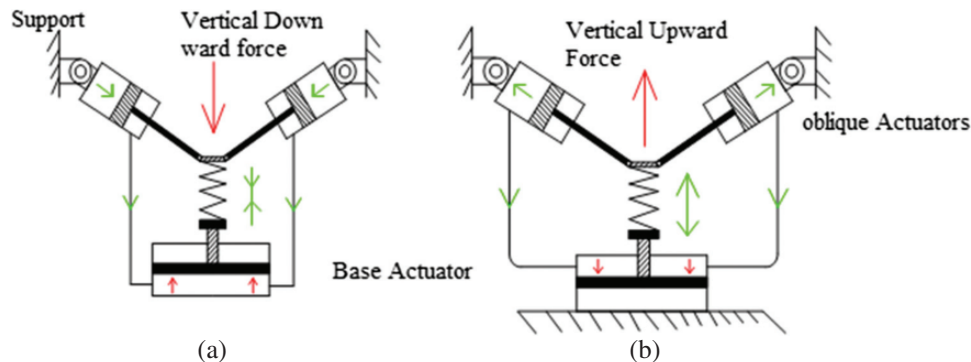


**Figure 2:** Dynamic response with applied force and excitation force

On the effect of applied force, it impinges on load base predominately and urges moving in downward vector as shown in Fig. 2(a), and prompts expansion in FA conjointly with angular displacement of FA setup by pivoted end. Thereupon the force transmitted as fluidic pressure from the compressed volume of FA on the piston rod side, the pressurized fluid from two FA enters into the cover side of the BA which tends to push the spring-base in upward vector, the helical coil spring is placed on spring-base to support load-base (between spring-base and load-base), similarly for base excitation it acts vice-versa. Since it is possible to fetch various isolation characteristics by experimenting with different springs and fluids that has different stiffness and bulk modulus respectively.

Let consider an analytical structure from Fig. 3 which shows the scheme of FA displacement action in symmetric. The continuous displacement of load-base effects to displace FA setup in angular by expansion of piston rod. To calculate the particular displacement values of actuators, load-base and piston rod with respect to applied static load range, it is important to compute the theoretical formulation.

#### 3.1 Static Analysis of QZS-FA Vibration Isolator

An isolator reacts with the various load range, which mitigates the induced amplitude by multiple absorbing techniques on load base. Initially, load-base responses with applied load as vertical

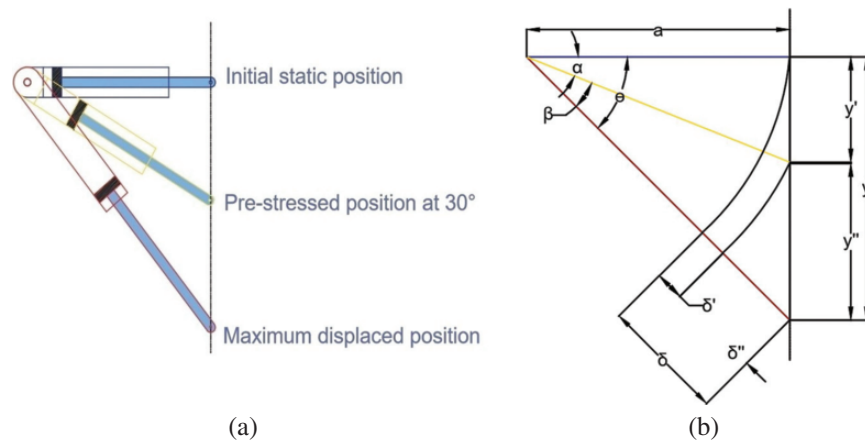


**Figure 3:** (a) Hydraulic actuator's displacement. (b) Line diagram with displacement

displacement, then deflection impinges on elements of an isolator as the compressive load on the helical coil spring and pulling force on oblique hanging FA. Theoretically the characteristics may obtain as (i) displacement characteristics and (ii) Load characteristics.

### 3.1.1 Displacement Characteristics

To achieve the better isolation efficiency the initial oblique setup should be kept at  $30^\circ$  for equal distribution of static force, accordance with Lamé's Theorem. The dynamic displacement characteristics of this pre-stressed position may obtain as sequence theoretical formulation of (i) Initial static position of FA as shown first position of an actuator in Fig. 3(a). (ii) Pre-stressed position as shown second and third position of an actuator in Fig. 3(a), and (iii) Constant pre-stressed position as 30 degree.

#### 3.1.1.1 Displacement Characteristics - FA at Initial Static Position as Zero Degree

Displacement ( $y$ ) Vs Angle ( $\Theta$ )

Vertical displacement of load base effects angular deflection on oblique actuator setup, from Fig. 3

$$y = a \tan \theta \quad (1)$$

Angle ( $\Theta$ ) Vs Deflection ( $\delta$ )

Angular deflection of actuator setup effects on actuator piston to displace or exert as shown in Fig. 4

$$\delta = a(\sec \theta - 1) \quad (2)$$

Displacement ( $y$ ) Vs Angle ( $\Theta$ ) Vs Deflection ( $\delta$ )

The relative motion of vertical displacement of load base with respect to angular deflection of actuator setup and piston displacement

$$y = (a + \delta) \sin \theta \quad (3)$$

#### 3.1.1.2 Displacement Characteristics – FA Among Pre-stressed Position

By insisting the pre-stressed position of the isolator to get an acquired non-linear characteristic the dynamic parameters correlation will be relationship between vertical displacement Vs Angle turned by oblique setup.

From Fig. 5 the following terms are can be considered

$$y = y' + y'', \delta' + \delta'' \text{ and } \theta = \alpha + \beta$$

from these relationships the Eq. 1 can become as

$$y' + y'' = a \tan \theta$$

$$y'' = a \tan \theta - y'$$

$$y'' = a \tan(\alpha + \beta) - a \tan \alpha$$

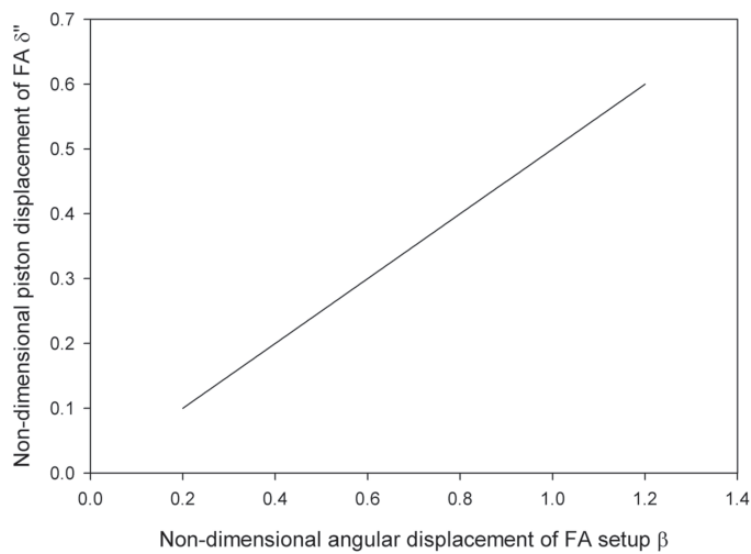


**Figure 4:** Piston displacement with angular displacement

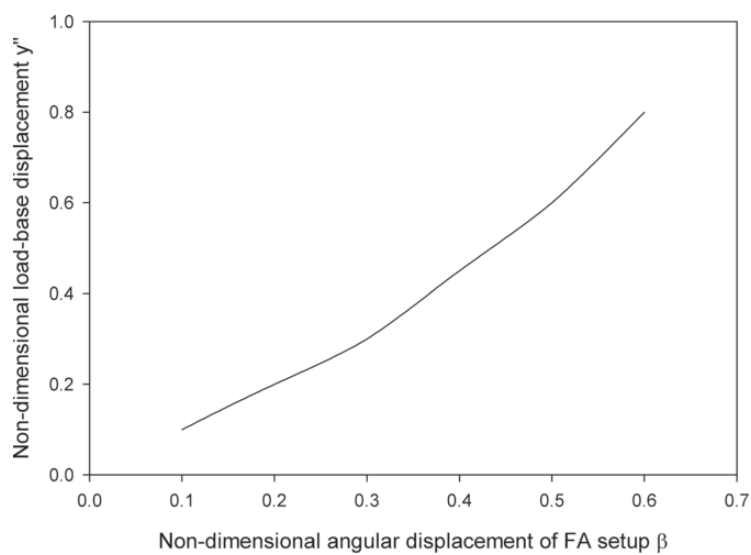


**Figure 5:** Angular deflection with load base displacement

$$y''(\alpha, \beta) = a \left[ \frac{\tan \alpha + \tan \beta}{1 - (\tan \alpha \tan \beta)} - \tan \alpha \right] \quad (4)$$

The relationship between piston displacement Vs angle turned by oblique setup

Eq. 2 by considering both initial and forced deflections

$$\delta' + \delta'' = a(\sec(\alpha + \beta) - 1)$$

$$\delta'' = a(\sec(\alpha + \beta) - 1) - a(\sec \alpha - 1)$$

$$\delta'' = (\alpha, \beta) = a[\sec(\alpha + \beta) - \sec \alpha] \quad (5)$$

The relationship between vertical displacement Vs angle turned by oblique setup and piston displacement

Eq. 3. by considering initial and forced deflections

$$y'' = (\alpha, \beta, \delta', \delta'') = (a + \delta' + \delta'')(\sin \alpha \cos \beta + \cos \alpha \sin \beta) - (a + \delta') \sin \alpha \quad (6)$$

### 3.1.1.3 Displacement Characteristics Among 30° Pre-stressed Position

By fixing the experimental setup initial expansion oblique angle as 30°, Vertical displacement of loadbase with function of angle turned by actuator setup

$$y''(\alpha = 30^\circ, \beta) = \frac{a}{\sqrt{3}} \left[ \frac{1 + \sqrt{3} \tan \beta}{1 - ((\tan \beta)/\sqrt{3})} - 1 \right] \quad (7)$$

The graph from Fig. 4, shows the variation in angular displacement of FA setup to the various vertical displacements of load base. From the graph the angular displacement of FA setup is increasing as the vertical displacement of load base increases. A gradual increase in angular displacement of FA setup occurs with proportionality constant (bulk modulus of fluid), initially the applied force acts on load-base and its effect both the FA setup oscillate, eventhough FA piston rod end pivoted at loadbase there is some time delay action due to bulk modulus and hence the slight decay of angular displacement of FA setup as shown in Fig. 4 for nondimensional angular displacement of 0.3 to 0.6 with respect to load base displacement.

Displacement of the piston due to angular displacement

$$\delta''(\alpha = 30^\circ, \beta) = \frac{2a}{\sqrt{3}} \left[ \frac{\csc \beta}{\cot \beta - 1/\sqrt{3}} - 1 \right] \quad (8)$$

The graph from Fig. 5 shows the piston displacement to the angular displacement of the actuator. As the angular displacement increases with respect to the piston displacement. Actually bulk modulus of fluid plays a main role in the displacement of the piston, but no need to consider an effect of bulk modulus for actuator displacement, because bulk modulus accounted in total displacement of load base and that total displacement is used to get angular displacement.

Vertical displacement with respect to angular displacement and piston movement

$$y''(\alpha = 30^\circ, \beta, \delta'') = \left[ \frac{a + a\left(\frac{2}{\sqrt{3}} - 1\right) + \delta''}{2} [\cos \beta + \sqrt{3} \sin \beta] - \frac{a}{\sqrt{3}} \right] \quad (9)$$

$$y'' = \frac{\delta''}{2} \left[ (\gamma_1 + 1)(\cos \beta + \sqrt{3} \sin \beta) - \gamma_1 \right]$$

Configurative parameters  $\gamma_1 = \frac{\delta''}{ca}$ ,  $\gamma_2 = \frac{y''}{ca}$ , numeric constant  $c=1.1547$  (it is taken to optimize the formulae structure).

$$\delta'' = y'' \left[ \frac{4\gamma_1}{\gamma_1^2 + 2\gamma_1 + 3 - \gamma_2^2} \right] \quad (10)$$

Theoretically, it is possible to compute the piston displacement with the effect of applied load, it will be directly proportional like angular displacement as shown in Fig. 6, it shows characteristics of isolator elements for a given load range as the variation in piston displacement to the various load conditions. As seen from the graph a steady increase in piston displacement occurred as the load increases for nondimensional piston displacement of 0.32 and afterthat a slight desplacement delay due to compressibility of fluid, from Fig. 6 clearly shows that, while fluid attains its maximum compressibility it acts as a solid member so the non dimensional displacement again started rising.

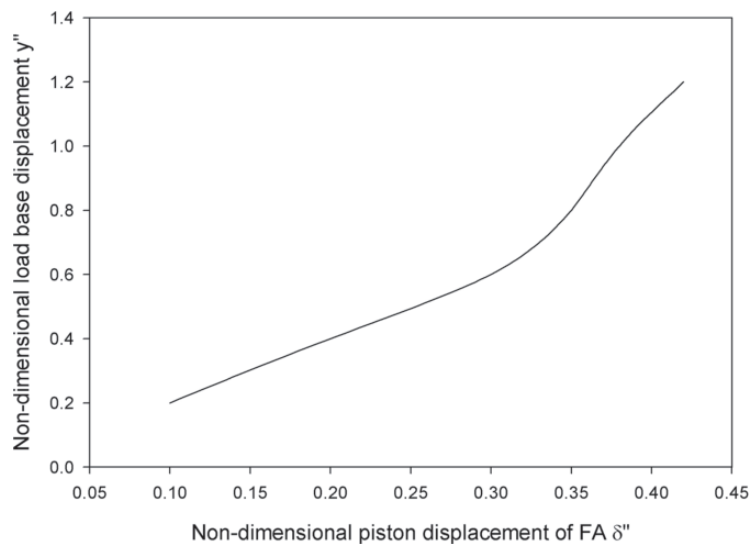


**Figure 6:** Angular response of actuators with respect to applied load

### 3.1.2 Load Characteristics

Total applied force is absorbed and supported by both spring stiffness and bulk modulus of the fluid  $(\Delta F) = \text{Load carried by spring stiffness } (F_s) + \text{Load carried by the bulk modulus of the fluid } (F_b) - \text{inverse restoring force by base actuator } (F_i)$

$$F = F_s + F_b - F_i \quad (11)$$

Total applied force is directly proportional to the vertical displacement of the loadbase

#### 3.1.2.1 Load Carried by Spring Stiffness ( $F_s$ )

Many researchers have designed the non linear vibration isolator with adjustable configurative parameters and formulated theoretical expression for force transmissibility [1-9]

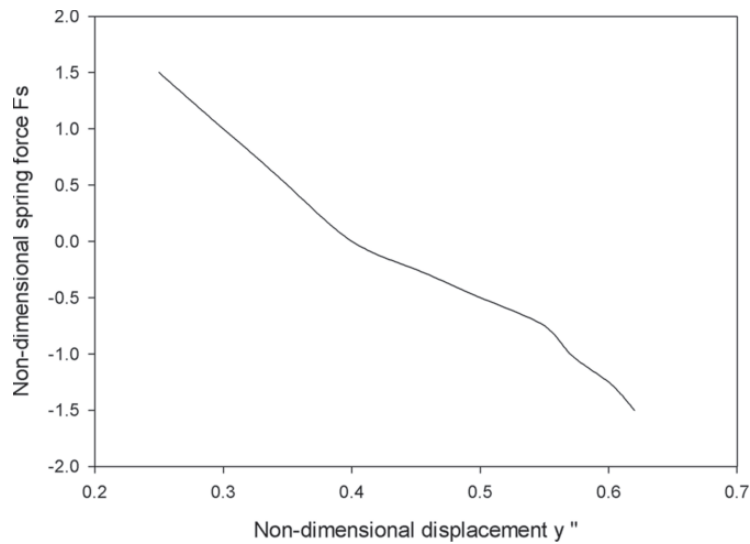


**Figure 7:** Load base displacement against spring stiffness with respect to Load

$$F_s = S \cdot y'' \quad (12)$$

The graph from Fig. 7, shows that the variation of non dimensional displacement of load-base against spring stiffness to the various loading conditions. Initially displacement against the spring stiffness reacts as constant up to solid length of the HCS and also reacts with base excitation amplitude by BA with this accordance the graph shows a minor displacement lag to absorb sudden impact.

### 3.1.2.2 Load Carried by the Bulk Modulus of the Fluid (Fb)

By the applications of Pascal's law, since hydraulic fluid is incompressible fluid. Even though the change in pressure leads to change in volume. But the stiff volume change may be confides on the elasticity of oil or compressibility of oil. Under the influence of the pressure, liquid behaves like a solid body and any change in pressure corresponds to the change in volume. Relative volume is directly proportional to the change in pressure

$$rv \propto \partial p \quad (13)$$

The bulk modulus plays a main role in pressure to volume transformation

$$rv = \frac{\partial p}{K} \quad (14)$$

Where relative volume  $rv = \frac{\partial V}{V}$

From Eqs. (13) and (14), the change in pressure effects to change in volume with respect to bulk modulus

$$\partial p = \frac{\partial V}{V} K \quad (15)$$

Elastic property of oil can be expressed by co-efficient of elasticity ( $E$ ) as the ratio between the change in force and change in compressive displacement

$$\frac{1}{E} = \frac{\partial F}{\partial x} = \frac{A \partial p}{\partial x} = \frac{A \frac{\partial V}{V} K}{\partial x} = \frac{AK}{x} = \psi K \quad (16)$$

$$\frac{A}{x} = \psi$$

The change in compressive displacement ( $\partial x$ ) of hydraulic cylinder when the pressure stagnated to absorb vibration.

$$\partial x = \frac{Fb}{E} = \frac{Fb}{\psi K} \quad (17)$$

Since change in piston displacement  $\partial x$  is piston displacement by bulk modulus  $\delta''$

Let consider the total volume of fluid reacts with bulk modulus on the both oblique fluidic actuators.

$$2 = \frac{Fb}{\psi K}$$

$$Fb = 2\psi K \quad (18)$$

From Eq. (10)

$$Fb = 2\psi K y'' \left[ \frac{4\gamma_1}{\gamma_1^2 + 2\gamma_1 + 3 - \gamma_2^2} \right] \quad (19)$$

The variation in non dimensional displacement against the bulk modulus of the fluid to the applied force has shown in Fig. 8. As the evidence from this figure the displacement against the bulk modulus is increase rapidly between 0.2 and 0.5 of Fb. After that the displacement against the bulk modulus has only the slightest increase up to the 0.8 Fb. This is because of load-base also reacts with the compressibility of fluid, which initially effects to fulfill the volume to maximum possible density, after that slightly responses to the applied load. The graphs from Figs. 7 and 8 depicts the variation of load base displacement against the stiffness of the spring and bulk modulus of the fluid to the applied load. As seen from the graphs, the displacement against the bulk modulus of the fluid is considerably less for various loads applied, a steady increase in displacement against the displacement of the spring is occurred to the various applied load, this is due to cumulative displacement with respect to applied load range by both spring stiffness and Bulk modulus of the fluid initially reacts and slightly absorbs with less amplitude of load base.

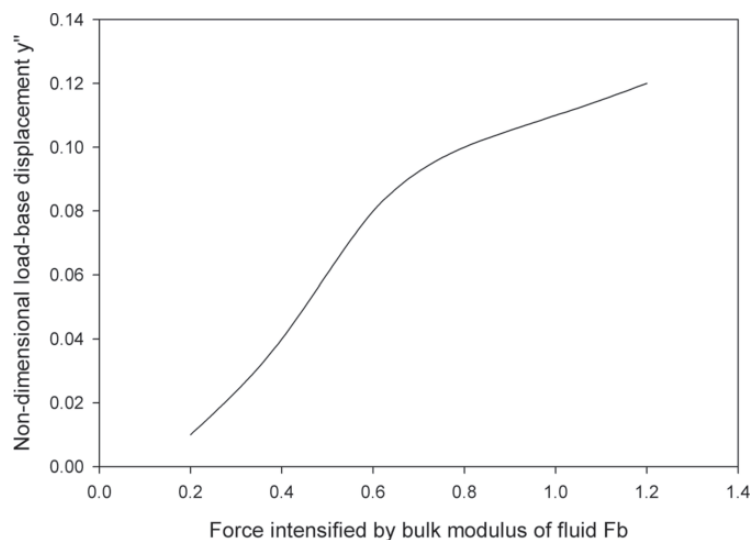


**Figure 8:** Load base displacement against bulk modulus of fluid with respect to load

3.1.2.3 Inverse Restoring Force by Base Actuator ( $F_i$ )

$$F_i = \psi K y' \tag{20}$$

Total restoring force

$$F = S y'' + 2\psi K y'' \left[ \frac{4\gamma_1}{\gamma_1^2 + 2\gamma_1 + 3 - \gamma_2^2} \right] - \psi K y' \tag{21}$$

We introduce the dimensionless parameters as follows

$$\hat{F} = \frac{F}{S}, \lambda = \frac{K}{S}$$

Where  $\lambda$  is the spring stiffness to fluid bulk modulus ratio,  $\hat{F}$  is the dimensionless restoring force. Thus, the dimensionless restoring force can be given by

$$\hat{F} = y'' \left[ 1 + \frac{8\lambda\psi\gamma_1}{\gamma_1^2 + 2\gamma_1 + 3 - \gamma_2^2} \right] - y' \lambda \psi \tag{22}$$

By differentiating Eq. (32) with respect to the dimensionless displacement  $\hat{y}$ , the dimensionless nonlinear stiffness  $\hat{K}$  of the system is obtained as [11]

$$\hat{K} = 2\hat{y} \left[ 1 + \frac{8\lambda\psi\gamma_1}{\gamma_1^2 + 2\gamma_1 + 3 - \gamma_2^2} - \lambda\psi \right] \tag{23}$$

It is also known as dimensionless nonlinear stiffness at the static equilibrium position. It can be seen that the value of  $\hat{K}$  is influenced by dimensionless parameters  $\hat{y}$ ,  $\lambda$  and adjustable configurative parameters and  $\psi$ , Fig. 9 depicts the dimensionless nonlinear stiffness curves for various parameters.

Maximum displacement is found at 1.2 having stiffness and restoring force approximates to 0.05 and 0.3 respectively. Minimum displacement is at 0.1 with the corresponding stiffness and restoring force as -0.28 and -0.5 respectively.

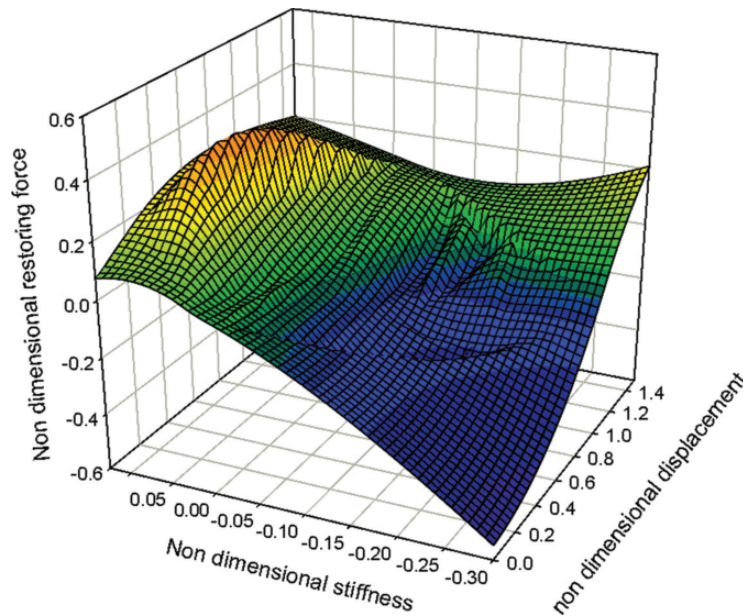


Figure 9: Comparative graph for non dimensional parameters

To simplify the subsequent dynamic analysis, the relationship between the restoring force and displacement is approximated by its seventh – order Taylor expansion at the static equilibrium [12]

$$\hat{F} = p\hat{y} + q\hat{y}^3 + r\hat{y}^5 + s\hat{y}^7 \quad (24)$$

Where  $p$ ,  $q$ ,  $r$  and  $s$  are the Taylor series derivative expansions of Eq. (22)

The seventh order Taylor expansion of the nonlinear stiffness is

$$\hat{K} = p + 3q\hat{y}^2 + 5r\hat{y}^4 + 7s\hat{y}^6 \quad (25)$$

### 3.2 Vibration Isolation Performance – Dynamic Analysis

The analytical model of QZS-FA vibration isolator system developed and its dynamic characteristics will be analyzed using averaging method. Dynamic equation with simple harmonic motion of a non linear vibration isolator can be given by [13]

$$m\ddot{y} + c\dot{y} + F = f \cos \omega t \quad (26)$$

where  $m$  is the mass,  $f$  and  $\omega$  are the amplitude and frequency of the harmonic excitation force respectively, and  $F$  is the restoring force as shown in Eq. (32).

Introducing the following dimensionless expressions

$$\omega_n = \sqrt{\frac{s}{m}}, \quad \xi = \frac{c}{2m\omega_n}, \quad \hat{f} = \frac{f}{s}, \quad \Omega = \frac{\omega}{\omega_n}, \quad \tau = \omega_n t \quad (27)$$

By considering all the dimensionless parameters Eq. (33) Can be written as

$$\hat{y}'' + 2\xi\hat{y}' + \hat{F} = \hat{f} \cos(\Omega\tau) \quad (28)$$

The averaging method can be used to solve Eq. (28)

$$\hat{y} = X \cos(\Omega\tau + \varphi)$$

$$\hat{y}' = -\Omega X \sin(\Omega\tau + \varphi)$$

$$\hat{y}'' = -\Omega X' \sin(\Omega\tau + \varphi) - \Omega^2 X \cos(\Omega\tau + \varphi) - \Omega X \varphi' \sin(\Omega\tau + \varphi)$$

$$X' = -X\xi - \frac{\hat{f} \sin \varphi}{2\Omega}$$

$$4\xi^2 X^2 - 4W\xi X + \hat{f}^2 = 0 \quad (29)$$

Assuming that the response is dominated by the fundamental harmonic response, the force transmitted to the base similar from [13]

$$\hat{f}t = \sqrt{-2\xi\Omega X \sin \Omega\tau + W \cos \Omega\tau + pX + qX^3 + rX^5 + sX^7}$$

$$\hat{f}t = \sqrt{(2\xi\Omega X)^2 + W^2 + pX + qX^3 + rX^5 + sX^7} \quad (30)$$

$$T = 20 \log_{10} \left( \frac{\sqrt{(2\xi\Omega X)^2 + W^2 + pX + qX^3 + rX^5 + sX^7}}{f_0} \right) \quad (31)$$

Figure 10 predicts the force transmissibility of the proposed system theoretically with approximate solutions considering with spring stiffness and damping factor of fluid. Since force transmissibility is depends with force transmitted to the foundation and applied force, it seems that for gradual increase in applied force the transmissibility first increase up to 1.2 (for system actuation) and then the transmissibility controlled with significant multi damping actions proposed in this system.

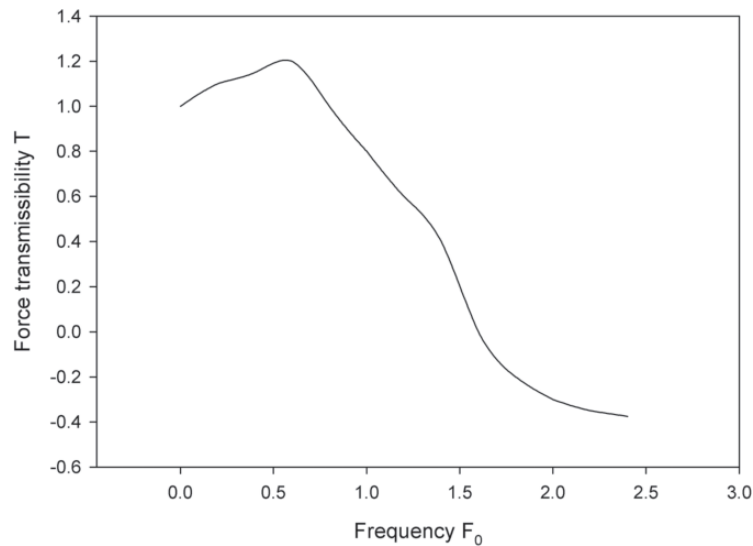


Figure 10: Analytical result of force transmissibility and frequency

#### 4 Modal Analysis

The modal analysis is performed to predict the structure vibration with standing capability and demonstrate the proposed model in to practical.

The vibration under damped condition is associated with

$$[M]y'' + [K]y' = 0 \quad (32)$$

$y$  is the mode displacement vector

$[M]$  is the mass matrix

The solution for free vibration will be harmonic and will be of the form,

$$\{y(t)\} = e^{\omega_i t} \{\phi\}_i$$

Where  $\{\phi\}_i$  is the Eigen vector with respect to  $i$ 'th natural frequency.

The first 5 Mode shapes for QZS-FA Vibration Isolator in estimated for different modal frequency with corresponding displacement in mm as stated in Tab. 1.

It is evident that from Tab. 1, the vibration frequency increases the displacement for corresponding frequency gets variation and obtained a maximum displacement with Mode 4. The analytical procedures carried to compare FEA and Analytical natural frequency, the determination of natural frequencies is obtain by [14]

**Table 1:** Modal frequency and displacement

Mode	Frequency (Hz)		Displacement (mm)
	FEA	Analytical	
1	42.8287	36.51	0.074
2	195.06	109.53	0.334
3	231.789	182.56	0.076
4	296.062	255.58	0.382
5	356.646	328.60	0.321

$$f_r = \frac{1}{2\pi} \sqrt{\frac{K_s}{m_{eq}}} \text{Hz} \quad (33)$$

Where,

$m_{eq}$  - Equivalent mass per area in  $\text{kg/m}^2$

$$m_{eq} = \rho * l$$

$\rho$  is the density of material  $7600 \text{ kg/m}^3$

$l$  is the stack length of load base  $0.02 \text{ m}$

$k_s$  is the spring stiffness coefficient,

$$K_s = \frac{192 * E * I}{l^3} \quad (34)$$

$E$  is the young's modulus

$I$  is the moment of inertia, given by

$$I = \frac{b * h^3}{12} \text{kg} \cdot \text{m}^2 \quad (35)$$

$b$  is the breadth of load base  $0.02 \text{ m}$

$h$  is the height of load base  $0.01 \text{ m}$

The Nodal solution for the harmonic analysis is performed by applying the unbalanced load to the load-base, in applied force and excitation force the maximum displacement as in Fig. 11 is obtained as  $0.170 \text{ mm}$ .

The harmonic analysis is predicted with the constraints of frequency limits as  $36 \text{ Hz}$  to  $350 \text{ Hz}$  with stepped procedure. It is obtained from Fig. 12(a), the displacement nearly to  $48 \text{ Hz}$  and  $410 \text{ Hz}$  is found to high approximated to  $4.1 \times 10^{-4} \text{ mm}$  and  $0.8 \times 10^{-4} \text{ mm}$  respectively, as in Fig. 12(a) similarly in Fig. 12(b) with  $50 \text{ Hz}$ ,  $360 \text{ Hz}$  and  $410 \text{ Hz}$  corresponding displacement is  $0.5 \times 10^{-4} \text{ mm}$ ,  $0.13 \times 10^{-4} \text{ mm}$  and  $0.95 \times 10^{-4} \text{ mm}$  respectively. The inference with modal and harmonic analysis in the machine should not operate with coincide of natural and vibrating frequency nearly equal to mode 1 and 5.

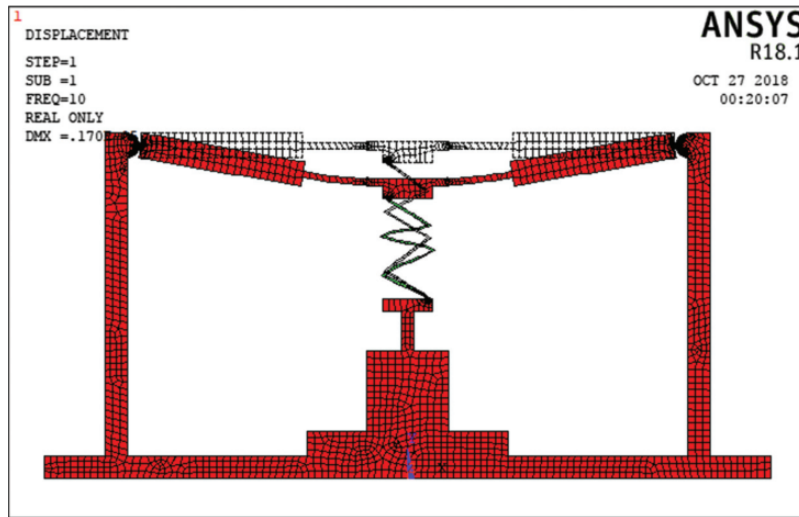


Figure 11: Counterplot of applied force

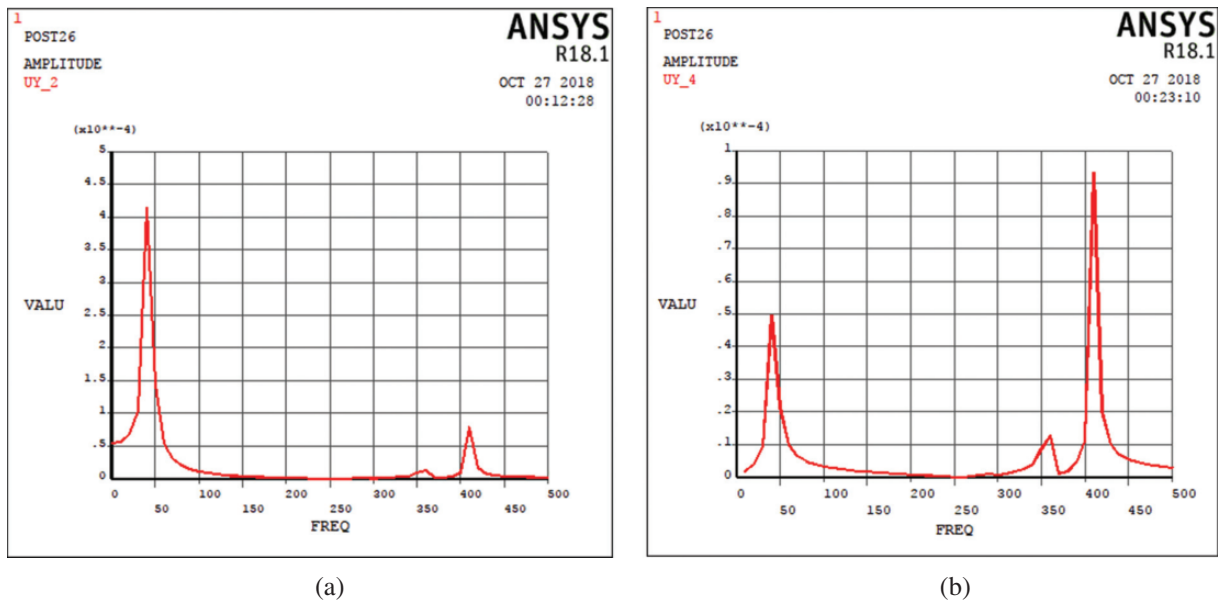
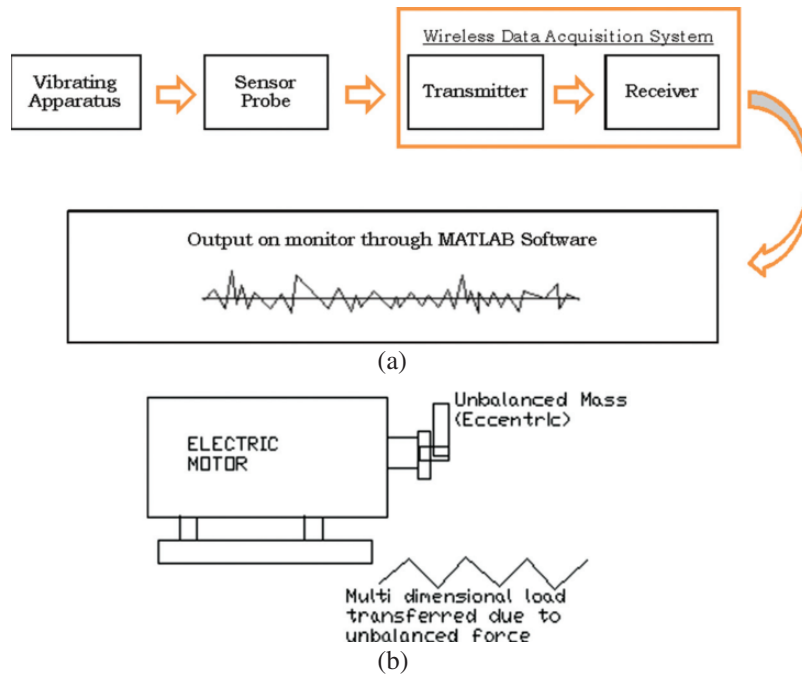


Figure 12: (a) Amplitude by applied force. (b) Amplitude by excitation force

## 5 Experimental Investigation

In recent technology many researchers are used different technology to predict vibration characteristics, from reviewing those techniques and openness this paper proposed a foolproof technique of wireless data acquisition system with accelerometer sensor probe, that was used here to predict vibration characteristics for NLVIFA.

The arrangement of experimental investigation compiled as shown in Fig. 13(a) as block diagram. Fig. 13(b) shows the pattern of inducing vibration by applying unbalanced force to the motor shaft.



**Figure 13:** (a) Block diagram of experimental setup. (b) Unbalanced load to load base

For experimentation purpose it is important to stimulate some vibration on the apparatus load-base, in this accordance an electric motor constructed with unbalanced eccentric loaded pulley was introduced and the same shown in Fig. 14(a)

The NLVIFA prototype primed, that was uniquely composed for the proposed system, suitable with non-dimensional physical parameters. An experimental setup for NLVIFA investigation has shown in Fig. 14(b).

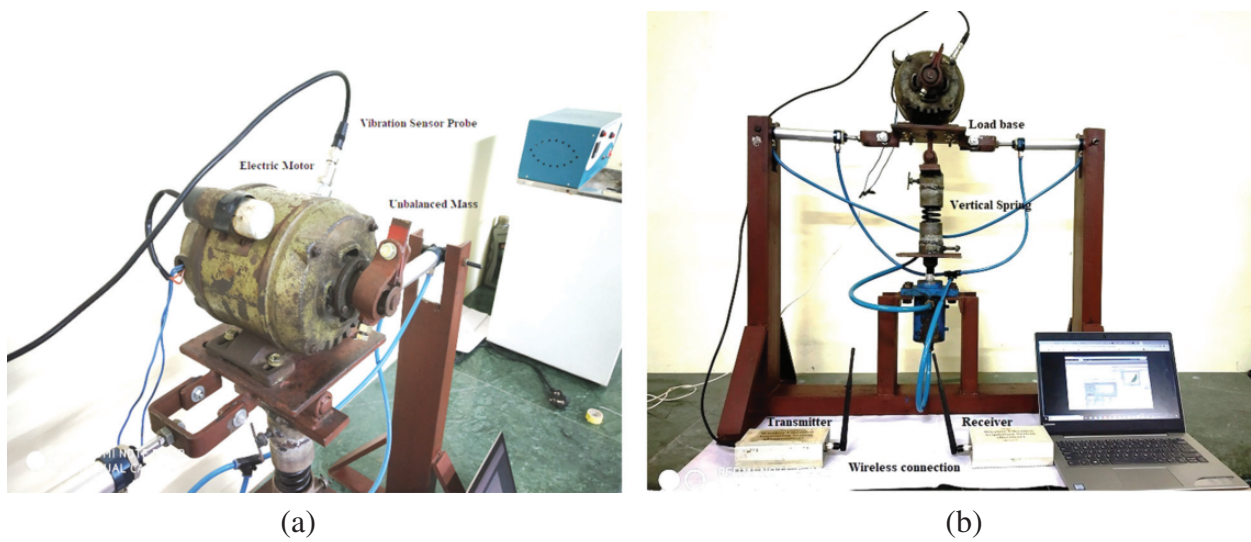


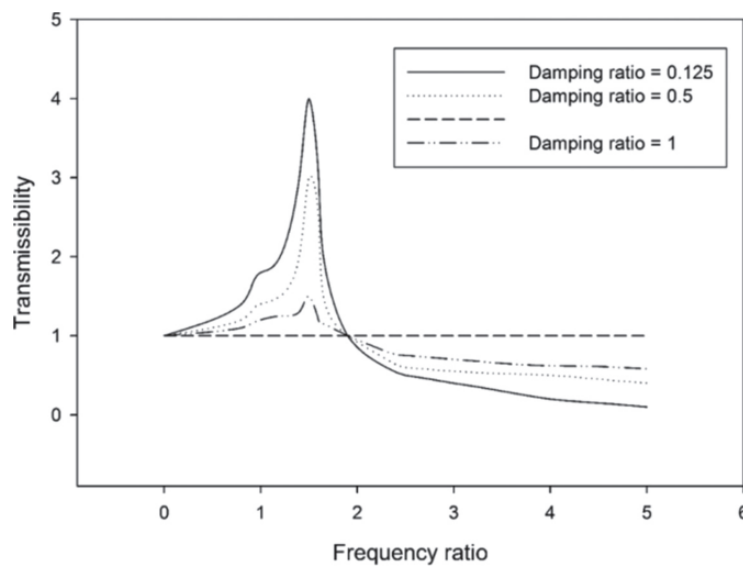
**Figure 14:** (a) Vibrating machine setup (eccentrically loaded electric motor). (b) Experimental setup of QZS-FA vibration isolator

The accelerometer sensor probe is attached to the vibrating apparatus as shown in Fig. 14(b) and transferring data to the wireless transmitter through cable, then the coded signal data transferred to the wireless receiver. After that wireless receiver transfers data to computer embedded with MATLAB software, finally the monitor displays the tailor made characteristics to predict the amplitudes and vibrational frequencies in the form of acceleration, and also the experimentation is carried with different bulk modulus fluid to investigate effect of damping in isolation performance.

## 6 Results and Discussions

The investigation of non-linear isolator characteristics exhibits under various damping condition to obtain better isolation with less amplitude. The fluid bulk modulus is utilized to suspend the rigidity structure of QZS-FA Vibration isolator.

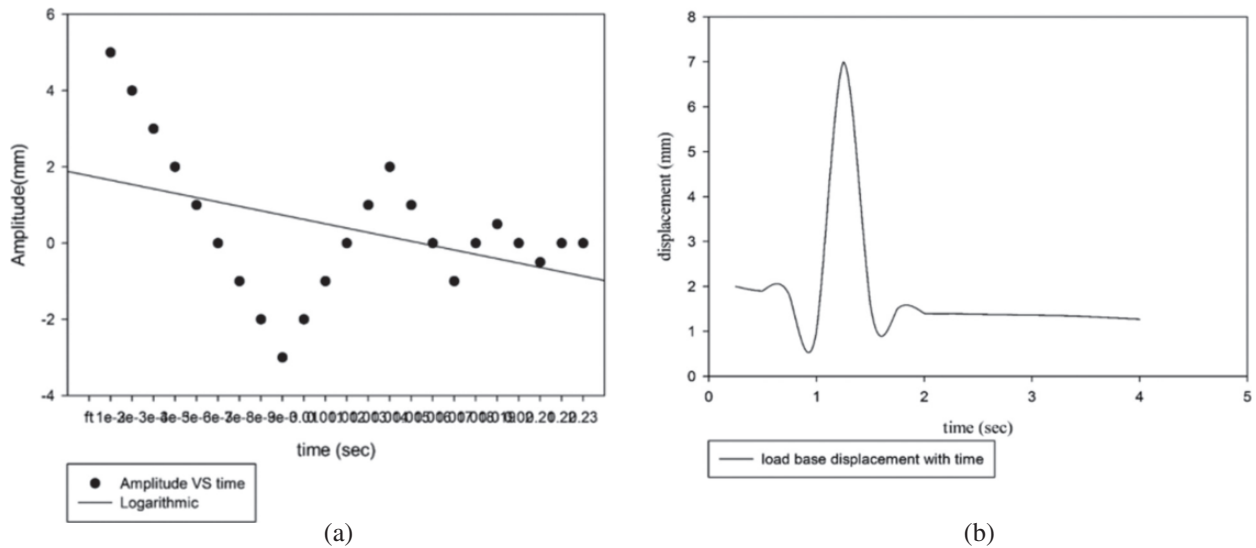
Figure 15 plots the transmissibility for various damping ratio achieved by changing different bulk modulus of fluids, here fluid compressibility property plays a vital role to absorb and suspend the dynamic imbalance as for low bulk modulus fluid of SAE 30 oil  $1.5 \text{ Nm}^{-2}$  inference the better solution at 0.125 damping ratio.



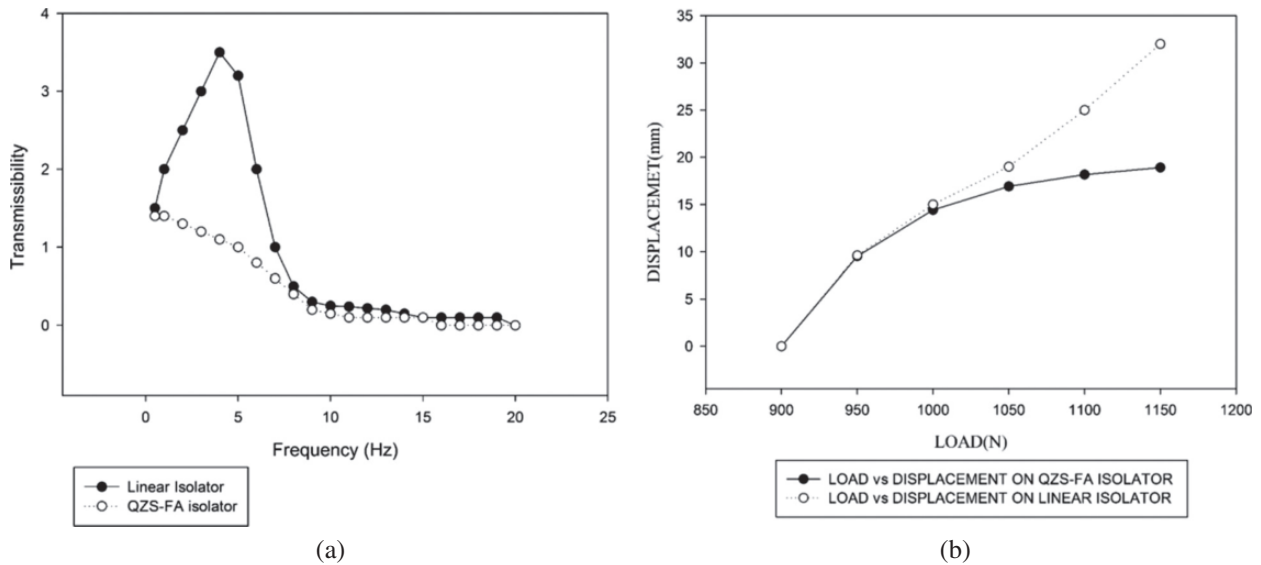
**Figure 15:** Transmissibility with various damping ratio

Figure 16(a) displays transient variation of amplitude having the higher value with initial to  $1 \times 10^{-2}$  seconds, and the logarithmic decrement plot show that the decay in vibrational amplitudes over time period decreased to every successive cycle (Fig. 16(b)). Plots the displacement of load base in time varying aspect found high in 1.2 seconds with 7 mm.

Figure 17(a) displays transmissibility for corresponding frequency for both linear and proposed isolator, it leads to the sudden increase of linear isolator transmissibility for initial frequency as decreases with increase in frequency. Fig. 17(b) compares the displacement with QZS-FA isolator with linear isolator; it is evident that the displacement of NLVIFA considerably low with the same load applied on linear isolator. This result shows an eminent promotion to the non linear isolator from coil spring mechanisms [7, 8]. The NLVIFA found to the decrease in transmissibility from increased to final frequency. So it is found that NLVIFA is superior to linear isolator. This is capable of isolating vibration between wide



**Figure 16:** (a) Excitation amplitude with time. (b) Excitation frequency with time



**Figure 17:** (a) Comparison of transmissibility. (b) Displacement comparison

range of external multi dimensional loads and base excitation. To attenuate external disturbance more at low and ultra low frequency with smoothness and without jerk by the aid of both helical coil spring stiffness and Bulk modulus of fluid. The quasi zero stiffness characteristic makes this NLVIFA reduce the external disturbance more at low frequencies, when compared with other type of isolators. And also deals with analysis of the effect of different loads and the implementation of auto adjustment by load action on base actuator.

Figure 18 shows the transient unbalanced motor frequency has higher acceleration at 3.58 seconds as  $42 \text{ m/s}^2$ .

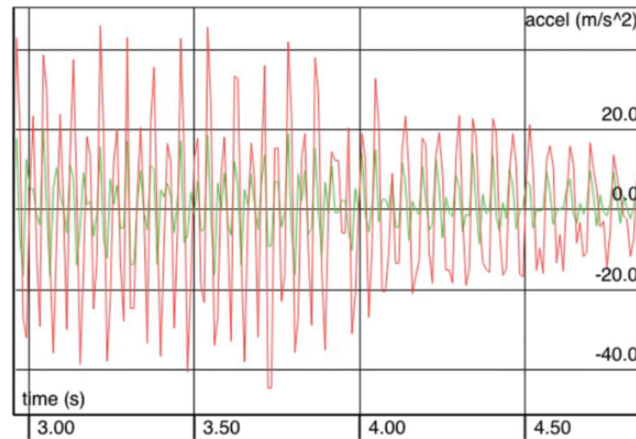


**Figure 18:** Un balanced motor frequency

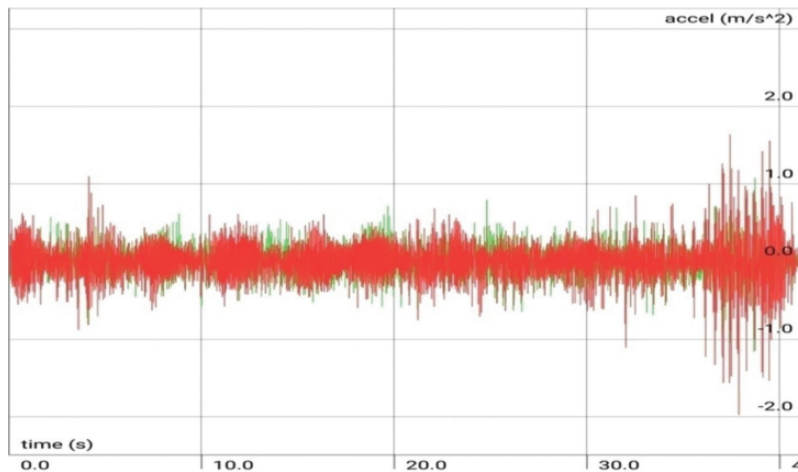


**Figure 19:** Experimental result of time – history diagram

The unbalanced motor (before mounting on QZS-FA Vibration isolator) frequency was comparably high with experimental setup made by [6, 14]. As before installation frequency of unbalanced setup has to be greatly controlled by proposed system.

Figure 19 shows the Experimental result of time – history diagram of the balanced load with QZS-FA Vibration Isolator results with a superior acceleration approximates at 38 seconds with  $1.5 \text{ ms}^{-2}$ . With reference to the Fig. 18 results the unbalanced system of  $40 \text{ ms}^{-2}$  acceleration decayed as time delayed active control of proposed system. This result shows an improvement in vibration isolation technology to reduce harmful vibration and higher base excitation effects. The proposed system gives better isolating performance on large excitation amplitude presence field impacts to reduce harmful vibrations. The experimental results comparing with theoretical results and modal analysis predicts the capability of NLVIFA system and also transmissibility characteristics, from this comparison it seems that theoretical response has slight change in significant performance with experimental one, which shows from Figs. 10 and 17(a), even though the transmissibility can be controlled by experimenting different bulk modulus fluids as varying different damping ratio. The suitability of all dynamic applications are mandatory, whereas the variation of load from low to high, when compares with Euler buckled beam nonlinear

isolator [9]. The complex phenomenon identified for the high static low dynamic system given by [2, 15] to explain zero stiffness as the minimum stiffness and negative stiffness controls the dynamic stiffness accordingly. Finally the proposed system having ability to perform under non-nominal loads and it can be adjustable with varying static load conditions by its self active inverse restoring force and also the system can be compatible with varying fluid and HCS to get significant applications from different loading conditions without disturbing its physical structure.

## 7 Conclusion

This research article investigates the non linear isolation behavior of NLVIFA system in theoretical and experimental manner significantly influences low vibration amplitude with unbalanced forces. The validation of NLVIFA correlates both FEA and numerical natural frequencies. The experimental results are compared to linear system observes that NLVIFA vibration isolator system violates the involvement of resonance phenomena and the performance for the proposed isolator can be extended to a lower frequency sphere and the adjustable damping ratio contributes the performance of an isolator with multiple phase applications without changing its compactness.

**Acknowledgement:** The authors are gratefully acknowledging the assistance of vibration analysis laboratory in Mechanical Engineering Department, Arunai Engineering College, Tiruvannamalai, Tamilnadu, India.

## References

1. Carrella, A., Brennan, M. J., Waters, T. P. (2007). Static analysis of a passive vibration isolator with quasi zero stiffness characteristics. *Journal of Sound and Vibration*, 301(3–5), 678–689. DOI 10.1016/j.jsv.2006.10.011.
2. Kovacic, I., Brennan, M. J., Waters, T. P. (2008). A study of a nonlinear vibration isolator with a quasi-zero stiffness characteristics. *Journal of Sound and Vibration*, 315, 700–711.
3. Yang, P., Yang, J., Ding, J. (2006). Dynamic transmissibility of a complex nonlinear coupling isolator. *Tsinghua Science and Technology*, 1, 538–542.
4. Ibrahim, R. A. (2008). Recent advances in nonlinear passive vibration isolators. *Journal of Sound and Vibration*, 314(3–5), 371–452. DOI 10.1016/j.jsv.2008.01.014.
5. Nataraj, M., Baskaran, G. (2017). Experimental investigation of misalignment and looseness in rotor bearing system using Bartlett power spectral density. *Journal of Scientific and Industrial Research*, 76(05), 308–313.
6. Sendhil Kumar, S., Senthil Kumar, M. (2014). Condition monitoring of rotating machinery through vibration analysis. *Journal of Scientific and Industrial Research*, 73(04), 258–261.
7. Sun, X., Xu, J., Jing, X., Cheng, L. (2014). Beneficial performance of a quasi-zero-stiffness vibration isolator with time delayed active control. *International Journal of Mechanical Sciences*, 82, 32–40. DOI 10.1016/j.ijmecsci.2014.03.002.
8. Lan, C. C., Yang, S. A., Wu, Y. S. (2014). Design and experiment of a compact quasi-zero-stiffness isolator capable of a wide range of loads. *Journal of Sound and Vibration*, 333(20), 4843–4858. DOI 10.1016/j.jsv.2014.05.009.
9. Huang, X. C., Liu, X. T., Hua, H. X. (2014). Effect of stiffness and load imperfection on the isolation performance of a high-static-low-dynamic-stiffness non-linear isolator under base displacement excitation. *International Journal of Mechanical Sciences*, 65, 32–43.
10. Xu, D., Yu, Q., Zhou, J., Bishop, S. R. (2013). Theoretical and experimental analyses of a nonlinear magnetic vibration isolator with quasi-zero-stiffness characteristic. *Journal of Sound and Vibration*, 332(14), 3377–3389. DOI 10.1016/j.jsv.2013.01.034.
11. Carrella, A., Brennan, M. J., Kovacic, I., Waters, T. P. (2009). On the force transmissibility of a vibration isolator with quasi-zero-stiffness. *Journal of Sound and Vibration*, 322(4–5), 707–717. DOI 10.1016/j.jsv.2008.11.034.
12. Le, T. D., Nguyen, V. A. D. (2017). Low frequency isolator with adjustable configurative parameter. *International Journal of Mechanical Sciences*, 134, 224–233. DOI 10.1016/j.ijmecsci.2017.09.050.

13. Wang, X., Liu, H., Chen, Y., Gao, P. (2018). Beneficial stiffness design of a high-static-low-dynamic-stiffness vibration isolator based on static and dynamic analysis. *International Journal of Mechanical Sciences*, 142, 235–244. DOI 10.1016/j.ijmecsci.2018.04.053.
14. Tang, Z., Pillay, P., Omekanda, A. M., Li, C., Cetinkaya, C. (2003). Measurement of Young's modulus for switched reluctance motor vibration determination. *IEEE Transactions on Industry Applications*, 38, 1027–1036.
15. Anvar, V., Alexey, Z., Artem, T. (2017). Study of application of vibration isolators with quasi-zero stiffness for reducing dynamics loads on the foundation. *Procedia Engineering*, 176, 137–143. DOI 10.1016/j.proeng.2017.02.281.